Some approximate methods for computing electromagnetic fields scattered by complex objects

Pierre Chiappetta, Bruno Torrésani

SOME APPROXIMATE METHODS FOR COMPUTING ELECTROMAGNETIC FIELDS SCATTERED BY COMPLEX OBJECTS

P. Chiappetta and B. Torrésani †
CPT, CNRS-Luminy, case 907, 13288 Marseille Cedex 09, France

Abstract. We discuss several approximate methods for computing electromagnetic scattering by objects of complex shape. Depending on the relative size of the scatterer compared to the incident wavelength, different techniques have to be designed. We review some of them which are often used in practice, and present numerical results of scattering by complex objects.

1. INTRODUCTION

The problem of electromagnetic scattering and absorption by objects of arbitrary shape and arbitrary internal structure is quite difficult and relies heavily on high-performance computing facilities. Exact solutions and algorithms exist for homogeneous particles of definite shape, such as spheres (Mie-Lorenz theory [1]), spheroids [2], cylinders [3]. For homogeneous particles algorithms also exist for circular disks [4], elliptical cylinders [5] and solids of revolution [6, 7, 8]. A few inhomogeneous objects such as layered spheres [9] can be treated as well.

The scattering by geometrically and electrically complex, three dimensional objects has driven an intensive effort to develop approximate numerical methods. The kind of approximation to be used depends highly on the characteristic lengths of the problem, and in particular on the dimensionless parameter ka, where k is the incident wavenumber and a a characteristic length of the scatterer. When $ka \ll 1$, *i.e.* for objects small compared to the incident wavelength, Born approximation provides satisfactory results. For larger sizes, the computation of scattering from complex three dimensional bodies involves the numerical solution of Maxwell's equations either in a differential form or in an integral form. For reasonable values of the parameter ka, say $ka \leq 5$, low frequency methods may be used. These methods are essentially based on a discretization of the scatterer, and a corresponding approximation of the electromagnetic field.

The discretization may be achieved in various ways (finite differences [10], finite elements [11, 12] (FEM), finite volumes (FVM), method of moments [13] (MoM), coupled dipoles (DDM),...) and in any case results in a large linear system to be solved numerically. Depending on the structure of the matrices obtained after discretization, several strategies may be followed for solving the numerical problem (for example direct inversions if the matrix is sparse enough, iterative schemes such as conjugate or biconjugate gradient methods (CGM), multigrid methods, FFT-based algorithms,...).

† Also at LATP, CMI, 39 rue F. Joliot-Curie, 13453 Marseille cedex 13, France.

For larger scatterers, such approximation methods are not suitable any more, in that they generally yield high dimensional matrix systems whose resolution with acceptable accuracy becomes untractable. In such situations, different types of approximations have to be designed, leading to various models such as eikonal models or asymptotic theories such as the geometrical theory of diffraction (GTD)[14, 15] or even geometrical optics. These approximations are essentially based upon a careful analysis of the oscillatory nature of the fields within the scatterer.

In the present contribution (which is rather a theoretical one) we aim at describing some of these approximation techniques and corresponding algorithms, focusing on a few ones which are relatively easy to implement practically. Our goal is *not* to provide an exhaustive account of existing approaches (this would deserve a several hundred pages contribution). Therefore, we apologize in advance for omitting a large number of significant contributions to the field which could easily find their place here.

Our discussion will be limited to the case of time-independent scattering. However, let us stress that the time-dependent case has been addressed by several authors as well, and that there exists an important literature on the subject. Some of the techniques we are about to review may be extended to the time-dependent situation. This is the case of finite elements methods for example. In this contribution, we refrain from discussing this more general problem.

This contribution is organized as follows. In section 2 we describe a couple of low-frequency approaches, namely the finite elements methods (FEM) and the coupled dipoles approximations (DDM) and variants. Section 3 is devoted to high-frequency approximations, with a special emphasis on eikonal methods. Section 4 is devoted to conclusions.

Throughout this contribution, we limit ourselves to the case of scattering of monochromatic waves for the sake of simplicity. By convention, we choose a dependence $E_0(\underline{r},t) = E_0 \exp\{i(\underline{k}.\underline{r} - \omega t)\}$ for the incident wave.

2. LOW-FREQUENCY APPROXIMATIONS

Let us start with the case of the scattering problem for scatterers whose size is of the same order as the incident wavelength (say, $1 \leq ka \leq 10$). As stressed in the introduction, several numerical strategies have been developed to address such a situation. Among them, integral formulations (integral forms of Maxwell's equations, finite elements, finite volumes...) are generally preferred, since they lead to algorithms which are more stable. Formulations based upon the integral form of Maxwell's equations are among the most popular. The three dimensional computer codes available are well adapted for prefectly conducting bodies [16], homogeneous dielectric bodies [17] of small or medium scale compared to the incident wavelength. The direct integral formulation does not seem to be well adapted to composite anisotropic and inhomogeneous scatterers. The advantage of the integral method is to take exactly the geometrical shape in account and the radiation condition is automatically enforced. The disadvantage is that the matrices involved are generally full, which is a severe limitation. Therefore, because of the strong demand for efficient algorithms capable of modeling complex and larger types of scatterer, there is room for alternatives. We describe essentially two of them here. The first one (the finite elements methods) is based on the mathematical theory of approximation, and expresses the fields as linear combinations of basis functions (finite elements) which span an approximation space

within which the solution is seeked. We cast it here as a low frequency method, but there is hope that it will allow one to address problems involving larger scales than the usual low frequency problems. The second approach (Discrete Dipoles Method) is rather based upon physical considerations, and approximates the scatterer as a superposition of spherical electric dipoles located on the sites of a (cubic) lattice. However, recent results have permitted to make the connexion with integral methods.

2.1. Finite Elements Methods.

2.1.1. Basics We consider the problem of the electromagnetic scattering within a bounded volume V. The considered volume V may contain various scattering objects such as metallic and resistive bodies, homogeneous or inhomogeneous dielectrics, all of which are arbitrarily shaped. The volume V is separated from the exterior domain by a surface $\Sigma = \partial V$ and we denote generically by $\hat{n}$ the exterior normal vector of length unity for each considered boundary. We denote by $\epsilon = \epsilon_0 \epsilon_r$ and $\mu = \mu_0 \mu_r$ the electric permittivity and magnetic susceptibility of the considered medium, and we use the subscript 0 to refer to free space and the subscript r to refer to relative characteristics of the medium. We also denote by $Z_0 = \sqrt{\mu_0/\epsilon_0}$ the impedance in free space.. The problem consists in solving the vector wave equation for the electric field, which reads in its most general form

$$\nabla \wedge (\frac{1}{\mu_r} \nabla \wedge E(\underline{r})) - k^2 \epsilon_r E(\underline{r}) = ikZ_0 J(\underline{r}) - (\nabla \wedge \frac{1}{\mu_r} M(\underline{r})) \tag{1}$$

where $k = \omega\sqrt{\mu_0 \epsilon_0}$ is the free space wave vector, and $J(\underline{r})$ and $M(\underline{r})$ denote the electric and magnetic current densities. The symbol $\wedge$ stands for the vector product in three dimensions Euclidean space. For the sake of simplicity, we shall refrain from considering the problem in full generality, and from now on we assume $J = 0$ and $M = 0$ in our discussion.

Trying to solve Eq. (1) pointwise turns out to yield numerically unstable algorithms. A standard alternative amounts to search for a "weak solution" of the problem, as follows. First, consider a family of vector basis functions $\Phi_\ell(\underline{r}), \ell = 1, \ldots L$ (the *test functions*), and impose eq. (1) in the sense of scalar products† with all basis functions $\Phi_\ell(\underline{r})$. Thanks to Green's equality, we end up with a system of L equations of the form

$$\begin{array}{l} \int_V \left[\frac{1}{\mu_r} (\nabla \wedge E(\underline{r})).(\nabla \wedge \overline{\Phi}_\ell(\underline{r})) - k^2 \epsilon_r E(\underline{r}) \cdot \overline{\Phi}_\ell(\underline{r}) \right] dv \\ \qquad = -ikZ_0 \int_\Sigma (\hat{n} \wedge H(\underline{r})) \cdot \overline{\Phi}_\ell(\underline{r}) ds \ . \end{array} \tag{2}$$

Here $H(\underline{r})$ is the total magnetic field satisfying Maxwell's equation:

$$\frac{1}{\mu_r} \nabla \wedge E(\underline{r}) = ikZ_0 H(\underline{r}) \tag{3}$$

To account rigorously for boundary conditions, equation (2) requires the knowledge of $\hat{n} \wedge H(\underline{r})$ on the boundary Σ, which itself requires solving the Stratton-Chu integral equation for $H(\underline{r})$:

$$\begin{array}{l} H(\underline{r}) = H^{inc}(\underline{r}) + \frac{ik}{Z_0} \int_\Sigma \underline{\underline{G}}(\underline{r}, \underline{r}').[E(\underline{r}') \wedge \hat{n}] \\ \qquad - \nabla \wedge \underline{\underline{G}}(\underline{r}, \underline{r}').[\hat{n} \wedge H(\underline{r}')] ds \end{array} \tag{4}$$

† That is, impose that for all $\ell = 1, \ldots L$, the scalar product of the left hand side with Φ_ℓ equals the scalar product of the right hand side with Φ_ℓ. By scalar product, we mean the Hermitian product on $L^2(\mathbb{R}^3, \mathbb{C}^3)$ defined by $\langle f, g \rangle = \int f(\underline{r}).\overline{g}(\underline{r}) d\underline{r}$ where the dot stands for Euclidean product in $\mathbb{C}^3$, and the bar denotes complex conjugation.

where $\underline{\underline{G}}(\underline{r},\underline{r}')$ is the free space matrix-valued Green's function (see eq. (25) below for its analytic expression). The solution of (2) and (4) corresponds to the *boundary integral formulation* (BI).

Alternatively, eq. (2) may be solved in an approximate way (without invoking the Stratton-Chu equation) by introducing artificial boundary conditions on $\Sigma = \partial V$. The simplest of such conditions is Sommerfeld's radiation condition (which is generally used at infinity), and has been extended by various authors to more general absorbing boundary conditions (ABC). Such conditions (see the discussion in section 2.1.3 below) relate the scattered electric and magnetic fields on the boundary Σ, and are therefore used to eliminate the magnetic field from (2). Doing so in the simplest case (i.e. with Sommerfeld's radiation condition, see eq. (10) below) for example, we are led to the following equation, in which only the scattered electric field is involved

$$\begin{aligned}\int_V [\frac{1}{\mu_r}(\nabla\wedge E(\underline{r})).(\nabla\wedge\overline{\Phi}_\ell(\underline{r})) - k^2\epsilon_r E(\underline{r})\cdot\overline{\Phi}_\ell(\underline{r})]dv \\ = -ikZ_0\int_\Sigma (\hat{n}\wedge H_0(\underline{r}))\cdot\overline{\Phi}_\ell(\underline{r})ds \\ - ikZ_0\int_\Sigma \hat{n}\wedge(\hat{n}\wedge(E(\underline{r})-E_0(\underline{r})))\overline{\Phi}_\ell(\underline{r})ds\end{aligned} \tag{5}$$

(we recall that $E_0(\underline{r})$ and $H_0(\underline{r})$ are the incident electric and magnetic fields respectively). Such a prescription (using Sommerfeld's condition or more general absorbing boundary conditions) is known under the name of ABC formulation.

To solve the weak forms of the wave equation, the next step is to introduce a second family of basis functions $\Psi_\ell(\underline{r})$ (the so-called *trial functions*), and to expand the electric field with respect to such a basis:

$$E(\underline{r}) = \sum_\ell e_\ell \Psi_\ell(\underline{r})$$

Therefore, eq. (2) transforms into a matrix equation, which is to be solved in order to yield the coefficients e_ℓ of the electric field. Clearly, the test and trial functions have to be chosen so as to make the numerical resolution as easy as possible. In that respect, the simplest choice is generally to use the same functions as test and trial functions. A general methodology for choosing such functions is based on finite elements decompositions of the volume V.

2.1.2. Finite elements The basis functions $\Psi_\ell(\underline{r})$ are generally constructed by discretizing the scattering volume, *i.e.* subdividing it into a finite number m_e of sub-elements V_e of definite shape such as rectangular bricks, tetrahedrals, triangular prisms... The associated surface elements are rectangles or triangles. The field within each element is expanded over basis functions $W_j^e(\underline{r}), j = 1,\ldots m_j$ depending on the geometry of the finite element:

$$E(\underline{r}) = \sum_{e=1}^{m_e}\sum_{j=1}^{m_j} E_j^e W_j^e(\underline{r}) \tag{6}$$

The unknown expansion coefficients E_j^e represent the electric field within the e-th element. The simplest choices for the basis functions $W_j(\underline{r})$ amounts to approximate the field within each volume V_e by a constant function. However, it is often desirable to work with higher order approximations. The next order is obtained as follows. For the

sake of simplicity, we limit ourselves to finite elements of rectangular shape. Consider a rectangular box V_e of sidelengths L_x, L_y and L_z respectively. Any component of the electric field $E^e(x,y,z)$ within V_e is projected onto the space spanned by four affine basis functions, which are taken to be functions of two variables only, so as to fulfill the zero divergence property of the electric field. For example, for the x component, one writes

$$E^e_x(y,z) = \sum_{j=1}^{4} E^e_{x;j} w^e_{x;j}(y,z) \ .$$

In such a simple case, we have to deal with 12 (scalar) basis functions within each element (note that with such a definition, the coefficients in the expansion coincide with the values of the field at the edges of the volume V_e). For example, for the elements $w_{x;j}(y,z)$:

$$\left\{ \begin{array}{lcl} w_{x;1}(y,z) & = & \frac{1}{L_y L_z}(L_y - y)(L_z - z), \\ w_{x;2}(y,z) & = & \frac{1}{L_y L_z} y (L_z - z); \\ w_{x;3}(y,z) & = & \frac{1}{L_y L_z}(L_y - y) z; \\ w_{x;4}(y,z) & = & \frac{1}{L_y L_z} yz, \end{array} \right. \tag{7}$$

and similar expressions for $w_{y,j}(x,z)$ and $w_{z,j}(x,y)$, $j = 1, \ldots 4$. Many other choices are possible and have been considered. For example, one can choose functions w^e such that the corresponding coefficients equal the values of the fields at the vertices of the finite elements grid. Alternatively, one can consider non-rectangular volumes, which allow one to accound more precisely for the geometry of the problem. We will not go into more details at this point. Let us nevertheless stress that whenever the solution is known to have a certain degree of smoothness, higher order schemes are expected to yield more precise approximations of the solution. Unfortunately, the implementation of higher order schemes is generally cumbersome, and lead to slowers algorithms. This is the usual precision-complexity tradeoff. For that reason, low order schemes are generally preferred.

Inserting the expansion (6) inside the integral equation of the electric field, for example eq. (5), yields a finite set of linear equations, which may be cast in the form

$$[\mathcal{M}^V] E^V_n + [\mathcal{M}^B] E^B_n = f^V_m \ , \tag{8}$$

where $\mathcal{M}^V$ and $\mathcal{M}^B$ are square matrices, and the superscripts B and V refer to fields E or matrices associated to the boundary surfaces (including the boundary $\Sigma = \partial V$ and all the boundaries of scattering elements within V) and the volume V respectively. The crucial point to notice is that because of the locality of finite elements and associated basis functions, all the matrices involved in (8) are sparse, which makes the numerical resolution much simpler.

On the contrary, if the exact BI formulation is used, one obtains a system of the form

$$[\mathcal{M}^V] E^V_n + [\mathcal{M}^B] E^B_n + [\mathcal{G}] E^B_n = f^V_m \ , \tag{9}$$

The extra term $[\mathcal{G}]$ comes from the presence of the Green's function in the Stratton-Chu equation (4). This introduces full matrices, since the decay of their elements is governed by that of Green's function, i.e. $1/r$, and is therefore generally quite unconvenient.

2.1.3. Boundary conditions To solve the scattering problem, it is necessary to specify the boundary conditions within the domain V and on its boundary Σ. Within the domain V, the boundary conditions are fixed by the physics, for example the vanishing of tangential electric field E for metallic bodies.

The conditions at the boundary $\Sigma = \partial V$ are generally more difficult. If the volume V is large enough and if Σ is far away from the scatterers, Sommerfeld's radiation condition

$$ikZ_0(\hat{r} \wedge H^{scat}(\underline{r})) = ikZ_0\hat{r} \wedge (\hat{r} \wedge E^{scat}(\underline{r})) \tag{10}$$

may be used (actually, Eq. (10) gives the so-called *Silver-Müller condition*, which has been shown to be equivalent to Sommerfeld's condition in [18]). Here, $\hat{r}$ is the normal to Σ, and $E^{scat} = E - E_0$ and $H^{scat} = H - H_0$ denote the scattered electric and magnetic fields respectively. But large domains require the use of a large number of finite elements, and lead to computer intensive algorithms, which turn out to be untractable in many situations of interest.

Absorbing boundary conditions (ABC) have been shown to provide useful alternatives. ABC methods basically aim at avoiding creating artificial backscatterings from the boundary Σ. An absorbing boundary condition of degree m is a relation between the scattered electric and magnetic fields that annihilates powers of $1/r$ of degrees up to $2m+1$ (Sommerfeld's condition is essentially an ABC of degree 0). We won't go into more details about ABC methods. Such methods have been extensively studied in the literature. We refer to [10, 19, 20, 21, 22, 23] for more details.

2.1.4. Numerical considerations and additional remarks As we have seen, whatever the exact formulation, we are in all cases led to solve numerically a linear system of high dimension. The resolution scheme has to satisfy two constraints: low computational cost, and low memory requirement. In principle, any direct or iterative scheme for such inversion would do the job equally well, but the latter are generally preferred because of their lower computational cost (see for example [24] for a review): they only require matrix-vector multiplications, and not matrix manipulations. For example, biconjugate gradient methods (BCG) have been extensively used, in different versions. These have $O(N^2)$ complexity.

In addition, the complexity may be significantly reduced if the matrices involved in the problem are sparse. Sparse matrices also reduce memory requirement if coded in an adequate way. As we have seen, all the matrices $[\mathcal{M}]$ involved in ABC method are generally sparse. This is no longer the case with the BI method, because of the matrix $[\mathcal{G}]$. However, such a problem may be reduced if the matrix $[\mathcal{G}]$ is block Toeplitz (which imposes uniform gridding). In such cases, Fast Fourier Transform algorithms may be used for evaluating $[\mathcal{G}]E_n^B$, imposing low memory requirement. Then the iterative methods mentioned above may be used. As shown in [21], the finite element method formulation is relevant for computation of electromagnetic scattering by complex and large non metallic three dimensional structures.

The main drawback of finite elements methods is their difficulty for accounting accurately for the surface termination of the finite element volume. Hybrid finite element-integral equation methods have been implemented [26]: the regions of material composition are handled with the finite element method (involving sparse matrices), whereas the structure of the surface is accurately treated using the exact boundary integral equation (requiring a full complex matrix for the surface). The

body size limitations are driven by computer speed and storage capacities. This method, previously restricted to dielectric bodies or aperture structures, has recently been extended [27] to many other types of scatterers (such as antennas, composite waveguides) by a curvilinear approach.

2.2. Coupled Dipoles and Related Methods.

We now turn to a different kind of approximation. In the same spirit as before, at low energies, the scattering and absorption cross sections can be obtained from a discretization of the scattering potential. Consider a scatterer, acted on by an incident beam, which is a linearly polarized electromagnetic field $E_0(\underline{r}) = E_0 \exp(i\underline{k}.\underline{r})$. The coupled dipole model (sometimes called discrete dipole model (DDM)) originates in a paper by Purcell and Pennypacker [28], and may be be briefly summarized as follows.

2.2.1. The Purcell-Pennypacker model In its simplest version, the dielectric scattering object is modelled by an array of polarizable elements, namely electric dipoles, located at the sites of a cubic lattice. Purcell and Pennypacker [28] used the Clausius-Mossoti (or Lorentz-Lorenz) prescription to assign polarisabilities to elementary volumes:

$$\alpha_e = \frac{3d_0^3}{4\pi}\frac{n^2-1}{n^2+2} \tag{11}$$

where n is the complex refractive index of the scatterer and d_0 the cubic lattice spacing. Each element at site i is given a dipole moment, proportional to the electric field at site i:

$$d_i = \alpha_e E_{eff}(\underline{r}_i) \tag{12}$$

where $E_{eff}(\underline{r}_i)$ is the superposition of the incident electric field and the electric field radiated by other sites:

$$E(\underline{r}_i) = E_0(\underline{r}_i) + E_{rad}(\underline{r}_i) = E_0(\underline{r}_i) + \sum_{j=1,j\neq i}^{N} T(\underline{r}_{ij}).d_j \tag{13}$$

The matrix T is given by

$$T(\underline{r}) = \frac{e^{ikr}}{r^3}[k^2r^2(1-\frac{\underline{r}\otimes\underline{r}}{r^2}) + (1-ikr)(3\frac{\underline{r}\otimes\underline{r}}{r^2}-1)] \ , \tag{14}$$

where the symbol $\otimes$ refers to Kronecker's product of vector: $(\underline{r}\otimes\underline{r}')_{ij} = r_i\, r'_j$. In other words, $\underline{r}\otimes\underline{r}/r^2$ is nothing but the orthogonal projection operator onto the line defined by $\underline{r}$.

This yields a system of $3N$ complex linear equations to be solved numerically. The method has been extended in many respects since then. More details are given below. Introducing the $3N \times 3N$ matrices $\mathbb{T}$ and $\mathbb{M}$

$$\mathbb{T}_{ij} = \alpha_e T(\underline{r}_{ij}) \, , \quad \mathbb{M} = 1 - \mathbb{T} \tag{15}$$

we are led to the following system of $3N$ complex linear equations to be solved numerically:

$$\mathbb{M}\,\mathbb{E} = \mathbb{E}_0 \ . \tag{16}$$

where $\mathbb{E}$ and $\mathbb{E}_0$ are the column vectors whose components are the values $E(\underline{r}_i)$ and $E_0(\underline{r}_i)$ of the fields at sites $\underline{r}_i$.

Assume for a while that the matrix equation (15) has been solved (more details are given in subsection 2.2.3 below). From the dipolar moments one gets the expressions for the integrated absorption and extinction cross sections:

$$\sigma_{abs} = 4\pi k \frac{\Im\,(\alpha_e)}{\mid \alpha_e \mid^2} \sum_{i=1}^{N} \frac{\mid d_i \mid^2}{\mid E_0 \mid^2} \tag{17}$$

$$\sigma_{ext} = -4\pi k \sum_{i=1}^{N} \frac{\Im\left(\exp(i\underline{k}.\underline{r}_i)\,\overline{d_i}.E_0\right)}{\mid E_0 \mid^2} \tag{18}$$

where $\Im(z)$ stands for the imaginary part of the complex number z. The differential cross sections are also easily computed by applying to the total dipolar moment $\sum_{i=1}^{N} d_i$ of the scatterer the asymptotic form of the matrix $T(\underline{r})$ i. e. :

$$T(\underline{r}) \to k^2 \frac{\exp(ikr)}{r}[1 - \hat{r} \otimes \hat{r}] \quad \text{as } r \to \infty \tag{19}$$

where $\hat{r} = \underline{r}/r$. The far field expression of the scattered field is then given by:

$$E(\underline{r}) = k^2 \frac{\exp(ikr)}{r} \sum_{i=1}^{N} \exp(-ik\underline{r}_i.\hat{r})[1 - \hat{r} \otimes \hat{r}].d_i \tag{20}$$

From eq. (20) one gets the differential scattering cross section:

$$\frac{d\sigma}{d\Omega} = \frac{P.\hat{r}}{\mid P_0 \mid} r^2 \tag{21}$$

where P (resp P_0) is the time averaged Poynting vector of the scattered (resp. incident) wave. The intensity functions, corresponding to different incident and scattered polarization states (hereafter denoted by ϵ_i and ϵ_s), can be computed from the formulae:

$$i_{\epsilon_i \epsilon_s}(\theta, \phi) = \lim_{r \to \infty} 2k^6 \left| \sum_{i=1}^{N} \exp(-ik\underline{r}_i.\hat{r})\, d_i.\ e_{\epsilon_s} \right|^2 \tag{22}$$

Here, the angles (θ, ϕ) are the spherical coordinates of the unit $\hat{r}$ vector. One is also interested in the corresponding ϕ averaged intensity functions:

$$i_{\epsilon_s}(\theta) = \frac{1}{2\pi} \int_0^{2\pi} i_{1\epsilon_s}(\theta, \phi)\, d\phi \tag{23}$$

This approach has been reconsidered by several authors (see [29] for a review of several variations), and has been shown to be particularly efficient in many situations. However, even though the approximation is physically clear and sound, it is not completely satisfactory mathematically since it is not derived from first principles (*i.e.* Maxwell's or Helmholtz's equations).

2.2.2. An alternative formulation The coupled dipole model may be justified in some sense as follows (see [30, 31, 32] for example). Start with the vector Helmholtz's equation, written in integral form

$$E(\underline{r}) = E_0(\underline{r}) - k^2 \int \underline{\underline{G}}(\underline{r} - \underline{r}')(1 - \epsilon(\underline{r}'))E(\underline{r}')d\underline{r}' \tag{24}$$

where $\underline{\underline{G}}(\underline{r})$ is the matrix-valued Green's function†, given by

$$\underline{\underline{G}}(\underline{r}) = \left(1 + \frac{1}{k^2}\nabla\nabla\right) G_0(\underline{r}) \tag{25}$$

$$= G_0(\underline{r}) \left(\left(1 - \frac{\underline{r} \otimes \underline{r}}{r^2}\right) - \frac{1}{k^2 r^2}(1 - ikr)\left(1 - 3\frac{\underline{r} \otimes \underline{r}}{r^2}\right) \right) - \frac{1}{3k^2}\delta(\underline{r}) \tag{26}$$

and $G_0(\underline{r})$ is the free space scalar Green's function

$$G_0(\underline{r}) = \frac{1}{4\pi}\frac{e^{ikr}}{r} \tag{27}$$

Inserting (25) into (24) yields the following integral equation:

$$\begin{aligned} &\tfrac{1}{3}(\epsilon(\underline{r}) + 2)E(\underline{r}) = E_0(\underline{r}) \\ &\quad - \tfrac{k^2}{4\pi}\int \tfrac{e^{ikr'}}{r'}(1 - \epsilon(\underline{r} - \underline{r}'))T(\underline{r}')E(\underline{r} - \underline{r}')d\underline{r}' \end{aligned} \tag{28}$$

Now we use the fact that we are at low frequency. The integration domain in (28) may be cut into small cubic subdomains of volume d_0^3 centered at sites denoted by $\underline{r}_j$, within which the integrand is approximately constant† (or may be replaced by some average value). Then we obtain the following expression for the electric field at site i:

$$\frac{1}{3}(\epsilon(\underline{r}_i) + 2)E(\underline{r}_i) = E_0(\underline{r}) + S_i + \sum_{j \neq i} \beta(\underline{r}_j)T(\underline{r}_j - \underline{r}_i)E(\underline{r}_j) \tag{29}$$

where S_i is the *self-interaction term* (see the discussion below), and

$$\beta(\underline{r}) = \frac{d_0^3}{4\pi}(\epsilon(\underline{r}) - 1) \ . \tag{30}$$

The self-interaction term has been carefully analyzed in [30]. It is easy to verify that for symmetry reasons, S_i is proportional to the field $E(\underline{r}_i)$. More precisely

$$S_i = \Gamma(d_0)\, E(\underline{r}_i) = \left(\int_{C_3(d_0)} \frac{e^{-ikr}}{r} d\underline{r}\right) \ E(\underline{r}_i) \ , \tag{31}$$

where $C_3(d_0)$ is the cube $[-d_0/2, d_0/2] \times [-d_0/2, d_0/2] \times [-d_0/2, d_0/2]$. $\Gamma(d_0)$ is a complex constant which may be computed numerically (see [30] for an estimate of its value). Therefore, up to minor modifications, we are again led to a problem similar to (16). The modifications concern both the self-interaction term, which modifies the denominator in the Clausius-Mossotti relation, and a coefficient in front of the incident electric field. We shall come back to these variations in subsection 2.2.5 below.

2.2.3. Numerical resolution Direct inversion of the matrix $\mathbb{M}$ is a cumbersome numerical problem, of complexity $O(N^3)$, and is better avoided. More reasonable numerical strategies rely on iterative schemes. The first attempt is due to Purcell

† Sometimes called a *dyadic Green's function [33]*. We recall that $\underline{\underline{G}}(\underline{r})$ is solution of $\nabla \wedge \nabla \wedge \underline{\underline{G}}(\underline{r}) - k^2\underline{\underline{G}}(\underline{r}) = \delta(\underline{r})$ and $\nabla.\underline{\underline{G}}(\underline{r}) = 0$, and satisfies Sommerfeld's radiation condition at infinity.

† This is nothing but the trapezoidal rule for evaluating the integral.

and Pennypacker, who proposed an iterative method based on alternate use of equations (12) and (13). Such a scheme may be proved to converge, but convergence may be rather slow. In fact, the method proved to be relevant in a number of situations [28], but sometimes suffers from unstable behavior as noticed by the authors.

Alternatively, Chiappetta [34] proposed to use the Neumann series $(1-\mathbb{T})^{-1} = 1+\mathbb{T}+\mathbb{T}^2+\mathbb{T}^3+\ldots$ to solve (15). For such a series to converge, the norm of $\mathbb{T}$ has to be smaller than unity (which is generally hard to verify *a priori*). This results in a multiple scattering expansion for the dipole moment at all sites

$$\begin{aligned} d_i &= d_{0i} + \alpha_e \sum_{j=1, j\neq i}^{N} T(\underline{r}_{ij}).d_{0j} \\ &+ \alpha_e^2 \sum_{j=1, j\neq i}^{N} \sum_{l=1, l\neq j}^{N} T(\underline{r}_{ij})T(\underline{r}_{jl}).d_{0l} + \ldots \ , \end{aligned} \tag{32}$$

which corresponds to a development on successive Born approximations. Here the subscript 0 refers to the Born term:

$$d_{0i} = \alpha_e E_{inc}(\underline{r}_i) \ . \tag{33}$$

The interesting point with such iterative schemes is that they never require matrix-matrix manipulations, but rather matrix-vector multiplication, which is of $O(N^2)$ complexity (instead of $O(N^3)$). This allows one to consider finer approximations for prescribed accuracy. Similar approach was followed by Singham and Bohren [35, 36] independently.

Other strategies have also been considered in the literature. Among iterative schemes, which are generally prefered (since they allow a significant reduction of computing time and memory storage), (complex) biconjugate gradient solvers (see e.g. [37, 24, 38] for a simple account) are among the most popular. Let us also quote fast Fourier transform (FFT) based algorithms, which may be used since the matrix $\mathbb{T}$ can be made block-Toeplitz, and lead to $O(N \log N)$ schemes. This is a significant improvement over iterative methods. Notice however that such an approach is possible only for regularly spaced dipoles in the scatterer, which forbids local refinements such as those examined in [39]. However, let us quote for completeness recent advances in FFT techniques, which make it possible to compute efficiently Fourier transforms for irregularly spaced data [40, 41], and could therefore allow combining FFT algorithms with adaptive gridding.

2.2.4. Numerical results The first test of accuracy of the coupled dipole method is the comparison to exact theories like spheres and spheroids. This has been done in [42] and several later references. In the case of spheres the comparison of the efficiency factors:

$$Q_i = \frac{\sigma_i}{A} \tag{34}$$

(where A is the geometrical cross section of the scatterer and i stands for extinction,absorption and scattered) exhibits a remarkable agreement with the Mie-Lorenz theory up to $ka = 2$. For a sphere of refractive index $n = 1.33 + 0.1i$ with $ka = 1.5$, which is modelled by 305 dipoles, the plot of intensity functions given in fig.1 show a very close agreement with exact calculation after 20 iterations.

We have also computed scattering by prolate spheroids and oblate spheroids for different values of the parameter $c = k\sqrt{a^2 - b^2}$ (a and b being the semi axis). The numerical results, shown in fig.2 for integrated efficiency factors and in fig.3 for intensity functions, fit fairly well exact results from Asano and Yamamoto [2]. The

coupled dipole model has been compared to experimental data on microwave scattering from a dielectric helix [43]. The right-handed seven turn helix of radius 1.83cm, wire radius 0.24cm and pitch 0.533cm, with refractive index $n = 1.626 + i0.012$ for an incident wavelength $\lambda = 3.18cm$ is modelled by an array of about 600 dipolar subunits. As shown in fig.4 the angular distributions of the intensity functions are in reasonable agreement with data. The cross polarized intensities i_{12} and i_{21} are found to be completely negligible, except in the case where the helical axis is in the scattering plane, perpendicular to the scattering vector. The predictions, given by our model, are closer to data than those obtained in [44].

2.2.5. Miscellaneous remarks The coupled dipole model has been studied by various authors, and modified at many points. One of the modifications concerns the point discussed in subsection 2.2.2, and leads to the so-called *digitized Green's funtion* (DGF) method [30]. This approach seems particularly interesting in that it derives the model from general principles, and not as an *ad hoc* model. Also, expressing the model an application of the trapezoidal rule to an integral equation, it suggests other possibilities for generalizations. For example, replace the trapezoidal quadrature with higher order ones, or adaptive integrators (which would be closer to the adaptive scheme suggested in [39]). Another interesting point in that this approach suggests that the Clausius-Mossotti prescription is not the best adapted one. This point also has been studied by various authors (see e.g. [29] for a review).

More recently, Lemaire [45, 46] generalized the coupled dipole approach in the following sense: each subunit is not only modelled by an electric dipole but also by an magnetic dipole and an electric quadrupole. Moreover, the Clausius-Mossoti expression for the polarisability being stricly valid only in the limit $kd_0 \to 0$, has been replaced by a more accurate expression given in [47] differing from inclusion of powers of kd and n. This model leads to more accurate results compared to Mie-Lorenz theory and allows to reach sizes up to $ka = 4.5$.

Other variations around this method may be found for example in [48, 49, 50].

3. HIGH-FREQUENCY APPROXIMATION

In the high frequency domain, the discretization techniques mentioned above don't apply any more, in the sense that the amount of data they would require would exceed by far the capabilities of all present time computers. However, other types of approximations may be used. These approximations are essentially based upon the fact that for scatterers large enough when compared to the incident wavelength, electromagnetic fields present fast oscillations, and are merely generalizations of Rayleigh-Gans and Van de Hulst scattering theories. The simplest of such asymptotic theories is the geometrical optics (or its quantum scattering equivalent, the WKB approximation), which has been refined to yield the geometrical theory of diffraction (GTD). GTD yields asymptotic expansions in powers of the frequency ω, which are generally truncated at the leading term (or at least the lowest order terms; in any case, the series is asymptotic and generally divergent). We shall not enter this subject here refering to [14, 15, 51] for detailed accounts. We rather focus on different approximations, inherited from quantum scattering theory, refered to as *eikonal approximations* from now on.

3.1. Scalar Eikonal Model

Our presentation follows essentially the discussion of [52], and is based upon the analysis of oscillatory integrals involved in the Lippmann-Schwinger equation. An alternative way to the eikonal model uses partial waves decomposition (see e.g. [53, 52, 54]). Let us first consider the scalar case, and denote by $\psi(\underline{r},t)$ the considered field. Our starting point is *Helmholtz's equation*, which for harmonic time dependence $\psi(\underline{r},t) = \psi(\underline{r})e^{-i\omega t}$ may be written as

$$\left(\Delta + k^2 n(\underline{r})^2\right)\psi(\underline{r}) = 0 \tag{35}$$

or, by setting $\mathcal{U}(\underline{r}) = k^2(1 - n(\underline{r})^2)$

$$\left(\Delta + k^2\right)\psi(\underline{r}) = \mathcal{U}(\underline{r})\psi(\underline{r}) \tag{36}$$

Setting $\psi(\underline{r}) = \varphi(\underline{r})\exp\{i\underline{k}\cdot\underline{r}\}$, the latter equation is conveniently rewritten as a *Lippmann-Schwinger equation* (which takes into account Sommerfeld's radiation condition as well):

$$\varphi(\underline{r}) = 1 - \frac{1}{4\pi}\int \frac{e^{i(kr''-\underline{k}\cdot\underline{r}'')}}{r''}\varphi\left(\underline{r}-\underline{r}''\right)\mathcal{U}\left(\underline{r}-\underline{r}''\right)d\underline{r}'' \tag{37}$$

We denote by $\underline{k}_r = k\underline{r}/r$ the diffracted wavevector. The asymptotic behavior of the field $\psi(\underline{r})$ is the following

$$\psi(\underline{r}) = 1 + f(\underline{k}_r,\underline{k})\frac{e^{ikr}}{r} + o\left(\frac{1}{kr}\right) \tag{38}$$

where the function $f(\underline{k}_r,\underline{k})$ is the *scattering amplitude*

$$f(\underline{k}_r,\underline{k}) = -\frac{k^2}{4\pi}\int e^{i(\underline{k}-\underline{k}_r)\cdot\underline{r}'}\mathcal{U}(\underline{r}')\varphi(\underline{r}')d\underline{r}' \tag{39}$$

Therefore, it may be seen from such an expression that in order to compute the scattered field at infinity, we need to know its expression within the support of the potential, *i.e.* inside the scatterer. When the wavenumber is large enough, it is possible to derive an approximate expression for $\varphi(\underline{r})$ inside the scatterer, as follows. Expressing the integration variable $\underline{r}''$ in (37) in polar coordinates $\underline{r}'' \sim (r'',\theta'',\phi'')$, set $\mu'' = \cos\theta''$. For the integration *wrt* μ, note that the integral is an oscillatory one. Using the integration by part lemma (see e.g. [55]), it is readily seen that up to terms of higher order in $1/(kr'')$, the integral is dominated by the contributions of integration bounds $\mu'' = \pm 1$. In addition, the bound $\mu'' = -1$ gives rises to another oscillatory integral when integrating *wrt* r''. Therefore at first order, one can focus on the first term, which yields (the integration *wrt* ϕ is a trivial one)

$$\begin{aligned}\varphi(\underline{r}) &= 1 - \frac{i}{2k}\int \varphi\left(\underline{r}-\underline{r}''\right)\mathcal{U}\left(\underline{r}-r''\underline{e}_z\right)dr'' \\ &= 1 - \frac{i}{2k}\int_{-\infty}^{z}\mathcal{U}(x,y,z'')\varphi(x,y,z'')dz''\end{aligned} \tag{40}$$

To evaluate the scattering amplitude, set now $\underline{r} = \underline{b} + z\underline{e}_z$. The variable $\underline{b}$ is called the *impact parameter*. Integration of equation (40) leads to the following expression for $\varphi(\underline{r})$:

$$\varphi(\underline{b}+z\underline{e}_z) = \exp\left\{-\frac{ik}{2}\int_{-\infty}^{z}\mathcal{U}(\underline{b}+z''\underline{e}_z)dz''\right\} \tag{41}$$

In terms of the impact parameter, the scattering amplitude reads:

$$f(\underline{k}_r, \underline{k}) = -\frac{k^2}{4\pi} \int \mathcal{U}(\underline{r}) e^{i(\underline{k}-\underline{k}_r)(\underline{b}+z\underline{e}_z)} e^{-i\frac{k}{2}\int_{-\infty}^{z} \mathcal{U}(\underline{b}+z''\underline{e}_z)dz''} d\underline{b}dz \tag{42}$$

Such an expression is suitable for numerical computations, since it essentially involves a Fourier transform. Notice that for homogeneous scatterer, *i.e.* for $\mathcal{U} = \mathcal{U}_0$ inside the scatterer, the eikonal function

$$\chi(z, \underline{b}) = \frac{k}{2} \int_{-\infty}^{z} \mathcal{U}(x, y, z'')dz'' \tag{43}$$

takes a simple form, since the primitive is simply equal to $\mathcal{U}_0 \ell(\underline{b}, z)$, where $\ell(\underline{b}, z)$ is the optical path inside the scatterer along the ray $\underline{b} + z'\underline{e}_z$, $z' \leq z$.

The expression in (42) may be simplified further if one assumes in addition that the potential has a revolution symmetry around the z axis. In such a case, setting $\mathcal{U}(b, z) = \mathcal{U}(\underline{b} + z\underline{e}_z)$, it is readily shown (see e.g. [34] for more details) that the scattering amplitude, which now only depends on the scattering angle θ, is given by

$$f(\theta) \approx -\frac{k^2}{2} \int_0^{\infty} J_0(kb \sin\theta) G(b) b db \tag{44}$$

where $G(b)$ is the *opacity function*, given by

$$G(b) = \int \mathcal{U}(b, z) e^{-2ik \sin^2\theta/2} e^{i\frac{k}{2}\int_{-\infty}^{z(b)} \mathcal{U}(b,z')dz'} dz \tag{45}$$

where $z(b)$ denotes the height of the boundary of the scatterer for fixed impact parameter b. Again, such an expression simplifies in the case of homogeneous scatterers, since the integral inside the scatterer is performed trivially. In order to account exactly for the shape of the scattering surface, one can first perform the integral over the z variable for a fixed value $b = b_0$. The problem is now to find the intersection points between the curve $b = S(z)$, where $S(z)$ is the equation of the boundary, and the line $b = b_0$. This may be done analytically for simple geometries, and numerically for more complex scatterers.

Notice also the solution proposed in [52], which yields further simplifications. Instead of expressing $\underline{r}$ as $\underline{r} = \underline{b} + z\underline{e}_z$, set $\underline{u} = (\underline{k} + \underline{k}_r)/|\underline{k} + \underline{k}_r|$ and $\underline{r} = \tilde{\underline{b}} + \tilde{z}\underline{u}$. Therefore, integration w.r.t. z becomes trivial, and equation (42) simplifies to

$$f(\underline{k}_r, \underline{k}) = -\frac{ik}{2\pi} \int e^{i(\underline{k}-\underline{k}_r)\underline{b}} \left(e^{i\chi(b)} - 1\right) d\underline{b}$$

where owing to (43) we have set $\chi(b) = \chi(\infty, b)$. Again, for simple potentials, the eikonal function and therefore the scattering amplitude may be computed explicitely.

3.2. Numerical examples

The consistency of the model has been extensively studied on simple geometries, such as spheres or spheroids. Since we are mainly interested in complex objects, we shall not report these tests here, and we refer to [56, 46] for a more complete discussion.

Scattering by rough particle is an important potential application of such approximation techniques. The use of eikonal methods for such a problem has been

considered in [57], where rugosity was modelled by a "fractal type" function† (see the upper right corner of fig.5 for the boundary's shape)., and in [58] for complex objects of different type. As shown in fig.5 the eikonal model predicts an important increase of the backscattered intensity. This trend is in qualitative agreement with experimental measurements of light scattering by a collection of large rough particles (see [60] and references therein). The strong oscillations predicted by the model have not been observed: this is not surprizing since the particles are not identical in shape and the angular resolution of the scattered intensity is much greater than the period of the predicted oscillations.

Different tests have been performed on particles whose surface section is made of quarter circles (a global three-dimensional shape of such an object is depicted in fig.6). The advantage of such a configuration is that such scatterers can be built and experimental data taken in the microwave range. As shown in figs 7 and 8 one sees the presence of strong oscillations, together with an increase of the backscattered intensity. Moreover one notices a correlation between the number of quarter circles appearing in the surface section $b = S(z)$ and the number of maxima of intensity in the angular domain $85° \leq \theta \leq 180°$, which can be interpreted as interference phenomena with a frequency of oscillations proportional to the distance between two elementary consecutive patterns.

An experimental check of the model in the microwave regime, using monostatic CW techniques, has only been performed for backscattered intensity [59] for E and H polarizations and different orientations of the scattering object. While relaxing the axial symmetry assumption is a straightforward extension (although it yields time consuming algorithms [61]), the main difficulty to confront the eikonal model to these measurements comes from the description of polarization effects. Without including those effects, a qualitative agreement, concerning the number of oscillations and the localization of the minima, with the component perpendicular to the scattering plane has to be noticed. For a sufficiently absorbing sphere, for which multiple reflections may be neglected, it has been shown [62] that the replacement of the coefficient in front of the opacity function :

$$\gamma(\theta) = \frac{1 - m^2}{4\sin^2(\frac{\theta}{2}) - (1 - m^2)} \tag{46}$$

by the coefficient of reflection:

$$r_1 = \frac{1 - a_0}{1 + a_0} \quad \text{with} \quad a_0 = \sqrt{(\frac{m^2 - \cos^2(\frac{\theta}{2})}{\sin^2(\frac{\theta}{2})})} \tag{47}$$

improves the eikonal formulation away from the forward direction. This analogy has been recently more systematically investigated [63, 64].

3.3. Miscellaneous remarks

One of the main shortcomings of the approach described above is the fact that a scalar model cannot account for polarization effects. Several attempts have been made in order to introduce polarization into the model, with only limited application range.

† Let us stress that the term "fractal" does not exactly match the mathematical definition. A fractal object is by definition self similar -in either a deterministic or in a probabilistic way-, which means that it is invariant upon arbitrary rescalings. Since we eliminate fluctuations over distances smaller than the incident wavelength, what we consider here is a (deterministic) fractal with cutoff.

A possible approach [61] amounts to generalize Van de Hulst's approximations to Mie-Lorenz theory. Mie-Lorenz theory expresses the diagonal components of the scattering matrix as linear combinations of Legendre polynomials. Using approximation techniques similar to those described above, it is easy to get "eikonal" forms for the coefficients of the expansion. The latter turn out to generalize to different geometries, such as spheroids or rough spheres. However, the generalization does not go beyond simple perturbations of spheres, which makes the approximation of limited practical interest.

A natural alternative amounts to start from vector Helmholtz's equations and seek a high frequency limit. To do that, let $E_0(\underline{r}) = \mathcal{E}_0 e^{i\underline{k}.\underline{r}}$ be the incident electric field. To describe polarization, it is convenient to introduce circular polarization vectors as follows. For a given wavevector $\underline{k}$, choose two perpendicular unit vectors $\underline{e}_1$ and $\underline{e}_2$, perpendicular to $\underline{k}$ and such that $\underline{k} = \underline{e}_1 \wedge \underline{e}_2$. The circular polarization vectors are defined by $\underline{e}_\pm(\underline{k}) = (\underline{e}_1 \mp i\underline{e}_2)/\sqrt{2}$. To emphasize the decomposition into the two polarization states, we write generically

$$E(\underline{r}) = E^{(\underline{k},+)}(\underline{r}) + E^{(\underline{k},-)}(\underline{r}) \ .$$

The far field expression for a given polarization state of the electric field reads

$$\begin{aligned} E^{(\underline{k},p)}(\underline{r}) &= E_0^{(\underline{k},p)}(\underline{r}) \\ &\quad + \tfrac{e^{ikr}}{r} \textstyle\sum_{p'=\pm} f(\underline{k}_r, p'; \underline{k}, p) \underline{e}_{p'}(\underline{k}_r) + o\left(\tfrac{1}{r}\right) \end{aligned} \tag{48}$$

where $f(\underline{k}_r, p'; \underline{k}, p)$ are the four components of the scattering amplitude, and read

$$f(\underline{k}', p'; \underline{k}, p) = \frac{1}{4\pi} \int \overline{E_0^{(\underline{k}',p')}}(\underline{r}) \mathcal{U}(\underline{r}) E^{(\underline{k},p)}(\underline{r}) d\underline{r} \tag{49}$$

Then the same strategy as before may be employed to evaluate the four scattering amplitudes. First, approximate the field within the scatterer from the vector form of Lippmann-Schwinger equation

$$E(\underline{r}) = E_0(\underline{r}) - \int \underline{\underline{G}}(\underline{r} - \underline{r}') \mathcal{U}(\underline{r}') E(\underline{r}') d\underline{r}' \tag{50}$$

(where $\underline{\underline{G}}$ is the dyadic Green's function given in (25)), using the fact that the prominent contribution comes from the forward direction. Then use the approximate expression within (49), to get approximate scattering amplitudes.

To our knowledge, such a method has not been used practically so far, and most of the literature focuses on the scalar case. However, it is clear now that vector formulations are needed.

4. CONCLUSIONS AND PERSPECTIVES

We have described in the present contribution a number of techniques for solving the scattering problem for complex objects. We have more especially focused on methods based upon approximations, rather than purely numerical approaches. As we have seen, the case of small scatterers is relatively simple to handle, and several powerful algorithms have been designed, based on various discretization schemes. The main limitation is a computational one. Discretization has to be achieved in such a way that the resulting algorithm has acceptable cost. In particular, full matrices have to be avoided as much as possible, unless they may be put in circulant form, suitable for

FFT-based techniques. This imposes severe limitations on the possible discretizations, as well as on the overall size of the considered scatterers compared to the wavelength.

For objects whose size is much larger than the incident wavelength (say $ka \geq 30$), asymptotic methods such as the geometrical theory of diffraction or some variants provide accurate asnwers, as long as the geometry of the scatterer is not too complex. Smaller values of the size parameter ka are also tractable using simpler techniques, for instance the eikonal approximations given above, but polarization effects still have to be analyzed carefully.

The main difficulties come from the intermediate domain, for which asymptotic methods are not appropriate, and low-frequency methods yield too large dimensional linear problems. However, it is reasonable to expect that the increase of computing power, together with recent advances in numerical algorithms [65, 66] will soon make it possible to address these problems in a satisfactory way.

REFERENCES

[1] G. Mie (1908): *Ann. Phys.* **25**, 377.
[2] S. Asano and G. Yamamoto (1975): *Appl. Opt.* **14**, 29.
[3] J. Wait(1955): *Can. J. Phys.* **33**, 189.
[4] H. Weil and C. M. Chu (1976): *Appl. Opt.* **15**, 1832.
[5] C. Yeh (1965): *J. Opt. Soc. Am.* **55**, 309.
[6] P. Barber and C. Yeh (1975): *Appl. Opt.* **14**, 2864.
[7] M. K. Iskander, A. Lakhtakia and C. M. Durney (1983): *IEEE Trans. Antennas and Prop.* **AP-31**, (1983) 317.
[8] T-K. Wu and L. L. Tsai (1977): *Radio Sci.* **12**, 709.
[9] A. L. Aden and M. Kerker (1951): *J. Appl. Phys.* **22**, 1242.
[10] R. Mittra (1990): *Partial Differential Equations Methods in Computational Electromagnetics*, in *Méthodes Asymptotiques et Numériques en Théorie de la Diffusion*, publication CEA-EDF-INRIA.
[11] G. Strang and S. Fix (1973): *An Analysis of the Finite Elements Method*, Englewood Cliffs, NJ, Prentice Hall.
[12] A. Bendali (1984): *Approximation par éléments finis de surface de Problèmes de Diffraction des Ondes Electromagnétiques*, Thèse de Doctorat d'état ès Sciences Mathématiques (in French), Université de Paris VI.
[13] E.H. Newman, K. Kingsley (1991): *J. Comp. Phys.* **61**, 1-18.
[14] J.B. Keller (1965): *J. Opt. Soc. Am.* **52**, 116.
[15] L.B. Felsen and N. Markuvitz (1973): *Radiation and Scattering of Waves*, Englewood Cliffs, NJ, Prentice Hall.
[16] D. R. Wilton, S. M. Rao and A. W. Glisson (1982): *IEEE Trans. Antennas Prop.* **30**, 409.
[17] K. Umashankar, A. Taflove and S. M. Rao (1986): *IEEE Trans. on Antennas and Prop.* **AP-34**, 758.
[18] W.K. Saunders (1952): *Proc. Nat. Acad. Sci.* **38**, 342-348.
[19] A. Bayliss and E. Turkel (1980): *Comm. Pure. Appl. Math.* **33**, 707
[20] A. Chatterjee and J. L. Volakis (1993): *Microwave Opt. Tech. Lett.* **6**, 886.
[21] J. L. Volakis, A. Chatterjee and L. C. Kempel (1994): *J. Opt. Soc. Am.* **11**, 1422.
[22] B. Engquist and A. Madja (1977): *Math. Comp.* **31**, (1977) 629.
[23] J. P. Webb and V. N. Kanellopoulos (1989): *Microwave Opt. Tech. Lett.* **2**, 370.
[24] J. Dongarra et al (1995): *Templates for Iterative Resolution of Linear Systems*, SIAM Editors.
[25] H.C. Van de Hulst (1957): *Light Scattering by Small Particles*, Wiley.
[26] K. D. Paulsen, D. R. Lynch and W. J. Strohbehn, IEEE Trans. Microwave Theory Tech. **36**, (1988) 682; X. Yuan, IEEE Trans. Microwave Theory Tech. **38**, (1990) 1053; J. M. Jin and J. L. Volakis, IEEE Trans. Antennas Prop. **39**, (1991) 1598.
[27] G. E. Antilla and G. Alexopoulos (1994): *J. Opt. Soc. Am.* **A11**, 1445.
[28] E. M. Purcell and C. R. Pennypacker (1973): *Astrophys. J.* **186**, 705.
[29] B. T. Draine and P. J. Flatau (1994): *J. Opt. Soc. Am.* **11**, 1491.
[30] G. H. Goedecke and S. G. O'Brien (1988): *Appl. Opt.* **27**, 2431.
[31] J.I. Hage, J.M. Greenberg (1992): *Astrophys. J.* **361**, 251-259.

[32] M.K. Iskander, H.Y. Chan, J.E. Penner (1989): *Appl. Opt.* **28**, 3083-3091.
[33] C.T. Tai (1993): *Dyadic Green's Functions and their Use in Electromagnetic Theory*, IEEE Press.
[34] P. Chiappetta (1980): *J. Phys.* **A13**, 2101.
[35] S. B. Singham and C. F. Bohren (1988): *J. Opt. Soc. Am.* **A5**, 1867.
[36] S. B. Singham and C. F. Bohren (1987): *Opt. Lett.* **12**, 10.
[37] W.H. Press, B.P. Flannery, S.A. Teukolsky and W.T Wetterling (1986): *Numerical Recipes*, Cambridge Univ. Press, Cambridge, England.
[38] J. Stoer and R. Bulirsch (1991): *Introduction to Numerical Analysis*, 2nd edition, Texts in Applied Mathematics 12, Springer Verlag .
[39] C. Bourrely, P. Chiappetta, T. Lemaire and B. Torrésani (1992): *J. Opt. Soc. Am.* **A9**, 1336.
[40] G. Beylkin (1995): *Appl. Comp. Harmonic Anal.* **2**, 363.
[41] A. Dutt and V. Rokhlin (1995): *Appl. and Comp. Harmonic Anal.* **2**, 85.
[42] P. Chiappetta, J. M. Perrin and B. Torrésani (1987):, *Nuovo Cimento* **9D**, 717.
[43] P. Chiappetta and B. Torrésani (1988): *Appl. Opt.* **27**, 4856.
[44] R. D. Haracz, L. D. Cohen, A. Cohen and R.T. Wang (1987): *Appl. Opt.* **26**, 4632.
[45] T. Lemaire (1997): *J. Opt. Soc. Am.* **A14**, 470.
[46] T. Lemaire (1990): *Contribution à l'étude de la diffusion électromagnétique par des particules diélectriques dans le cadre d'approximations hautes et basses fréquences* PhD Thesis, Marseille (in French).
[47] B. T. Draine and J. Goodman (1993): *Astrophys. J.* **405**, 685.
[48] B. T. Draine (1988) *Astrophys. J.* **333**, 848.
[49] P. Flateau (1997): *Improvements of the Discrete Dipoles Approximation Methods*, Preprint, Scripps Institution, University of California, San Diego.
[50] J. J. Goodman, B. T. Draine and P. J. Flatau (1991): *Opt. Lett.* **16** 1198.
[51] R. Mittra ed. (1975): *Numerical and Asymptotic Techniques in Electromagnetics*, Springer Verlag.
[52] R. Newton (1982): *Scattering Theory of Waves and Particles*, 2nd edition, Texts and Monographs in Physics, Springer Verlag.
[53] R.J. Glauber (1958): *Lectures in Theoretical Physics 1*, W.L. Brittin and L.G. Dunham Eds., Interscience.
[54] P. Chiappetta (1980): *Astronomy and Astrophysics* **83**, 348.
[55] E. Copson (1965): *Asymptotic expansions*, Cambridge University Press.
[56] P. Chiappetta and J.M. Perrin (1985): *Optica Acta* **32**, 907-921.
[57] C. Bourrely, P. Chiappetta and B. Torrésani (1986): *J. Opt. Soc. Am.* **A3**, 250.
[58] C. Bourrely, P. Chiappetta and B. Torrésani (1986): *Opt. Comm.* **58**, 365.
[59] R. Deleuil (1969): *Optica Acta* **16**, 23.
[60] K. Weiss-Wrana (1983): *Astron. & Astrophys.* **126**, 240.
[61] C. Bourrely, P. Chiappetta and T. Lemaire (1991): *J. Mod. Opt.* **38**, 305.
[62] J.M. Perrin and P.L. Lamy (1983): *Optica Acta* **30**, 1223.
[63] C. Bourrely, P. Chiappetta and T. Lemaire (1996): *J. Mod. Opt.* **43**, 409.
[64] J.M. Perrin and P.L. Lamy (1986): *Optica Acta* **33**, 1001.
[65] B. Bradie, R. Coifman and A. Grossmann (1993): *Appl. and Comp. Harmonic Anal.* **1**, 94.
[66] V. Rokhlin (1993): *Appl. and Comp. Harmonic Anal.* **1**, 82

Figure Captions

Fig.1 Angular distributions of the intensity functions $i_1(\theta)$ and $i_2(\theta)$ for a sphere of size $ka = 1.5$ and index of refraction $n = 1.33 + i0.1$. Solid curve:Mie-Lorenz result. Dashed curve: coupled dipole method.

Fig.2 Scattering efficiencies Q_{sca} as a function of the excentricity c for spheroids of refractive index $n = 1.33$. Full curve: prolate spheroid with $\frac{a}{b} = 10$. Dashed curve: prolate spheroid with $\frac{a}{b} = 5$. Small dashed curve: prolate spheroid with $\frac{a}{b} = 2$, for several values of the incidence angle ζ. Dot dashed curve: oblate spheroid with $\frac{a}{b} = 2$.

Fig.3 Angular distributions of the intensity functions $i_1(\theta)$ (full curve) and $i_2(\theta)$ (dashed curve) for prolate spheroids of refractive index $n = 1.33$, with $\frac{a}{b} = 2$ for different c values: $c = 1, 2, 3, 4, 5$.

Fig.4 Angular distributions of the intensity functions $i_{11}(\theta)$ (full curve) and $i_{22}(\theta)$ (dashed curve) for a right-handed seven turn helix of radius 1.83cm, wire radius 0.23 cm and pitch 0.553 cm, with a refractive index $n = 1.626 + i0.012$ at the wavelength $\lambda = 3.18$ cm, placed in the scattering plane, perpendicular to the incident beam.

Fig.5 Differential cross-section $i(\theta)$ for a "fractal" particle of mean radius $a = 50\mu m$ and refractive index $n = 1.1 + i5.10^{-3}$, at the wavelength $\lambda = 0.62328\mu m$, as a function of the scattering angle θ. Solid line: object whose boundary is described at the top of the figure. Dashed curve: perfect sphere of same average radius and refractive index.

Fig.6 Global 3-dimensional shape of an object made of quarter circles.

Fig.7 Differential cross-section $i(\theta)$ for an object made of 8 quarter circles of average radius $a = 8cm$ and refractive index $n = 1.89 + i10^{-2}$ at the wavelength $\lambda = .86cm$. Solid line: object whose boundary is described at the top of the figure. Dashed curve: perfect sphere of same average radius and refractive index.

Fig.8 Differential cross-section $i(\theta)$ for an object made of 16 quarter circles of average radius $a = 8cm$ and refractive index $n = 1.89 + i10^{-2}$ at the wavelength $\lambda = .86cm$.

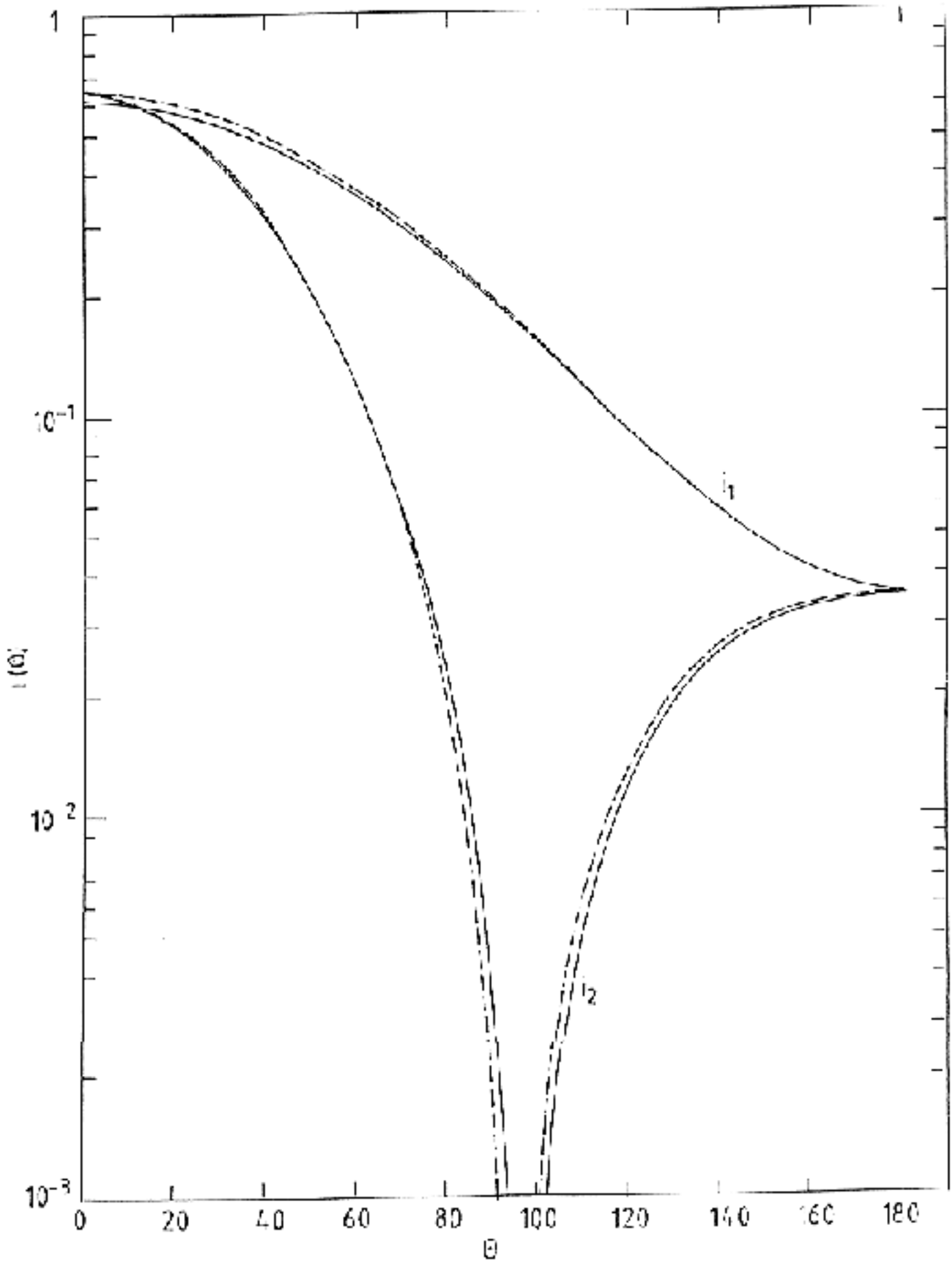

FIGURE 1

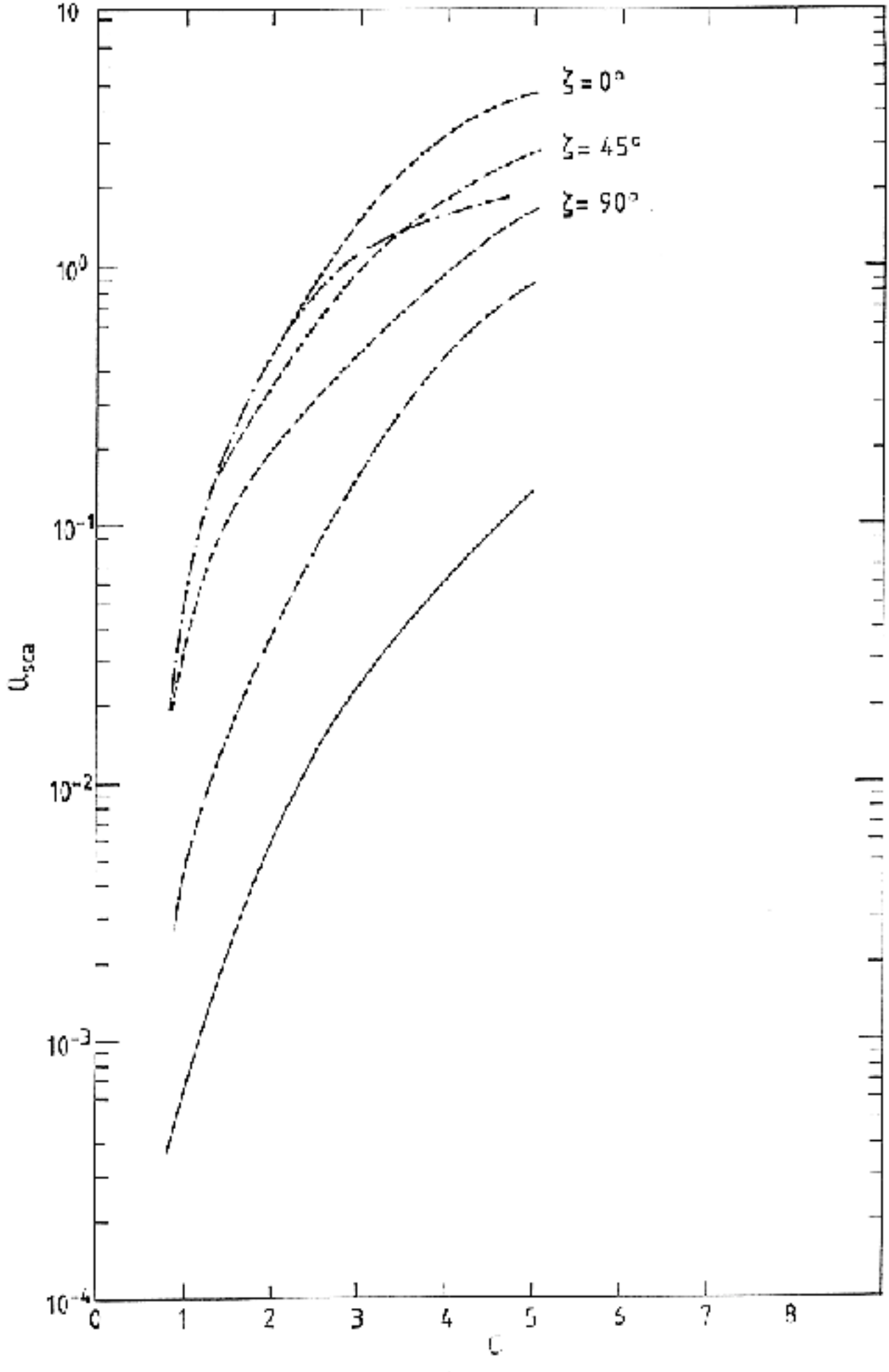

FIGURE 3

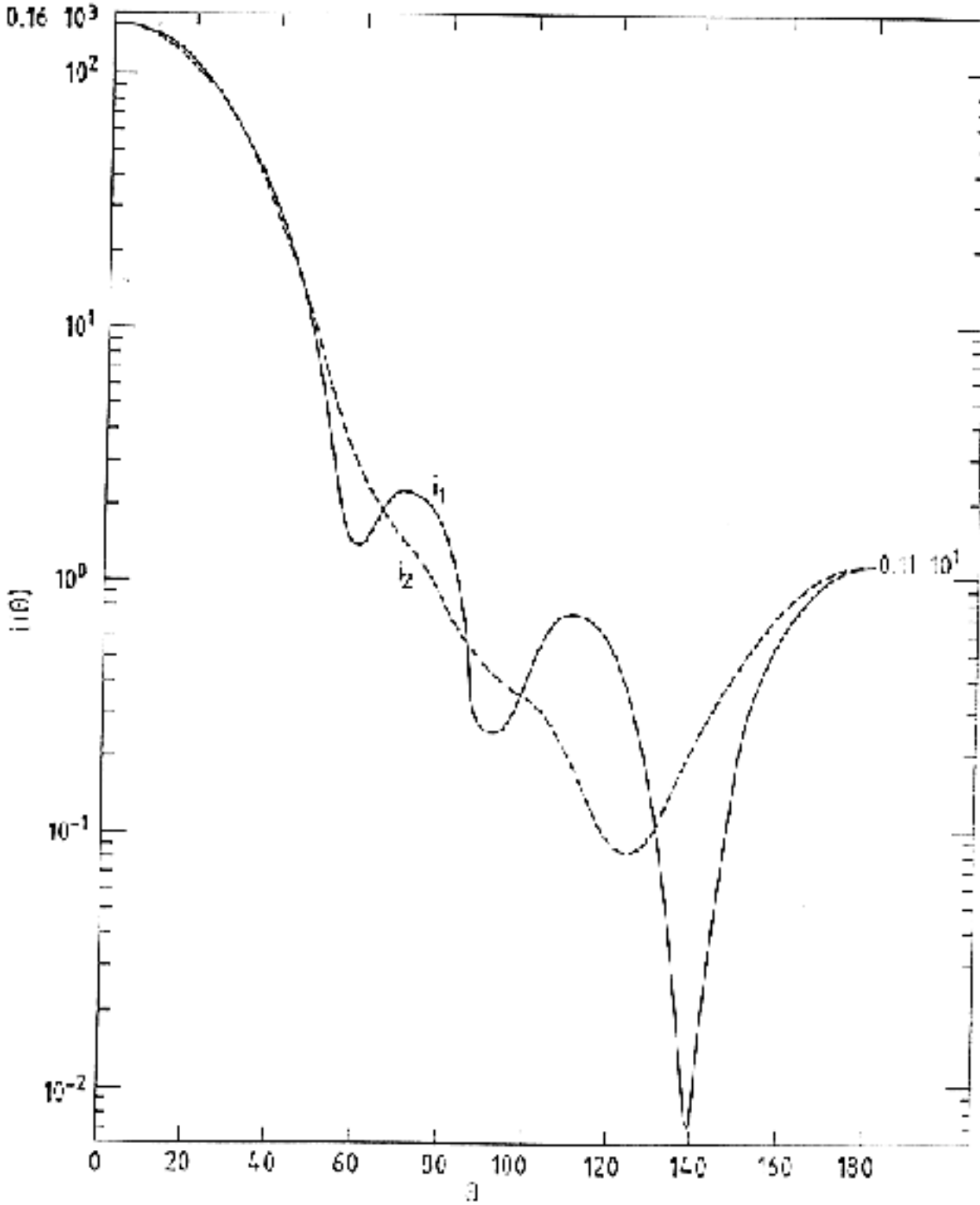
0.16 10³
10²
10¹
10⁰
10⁻¹
10⁻²
i(θ)
i1
i2
0.1 10¹
0
20
40
60
80
100
120
140
160
180
θ

FIGURE 3

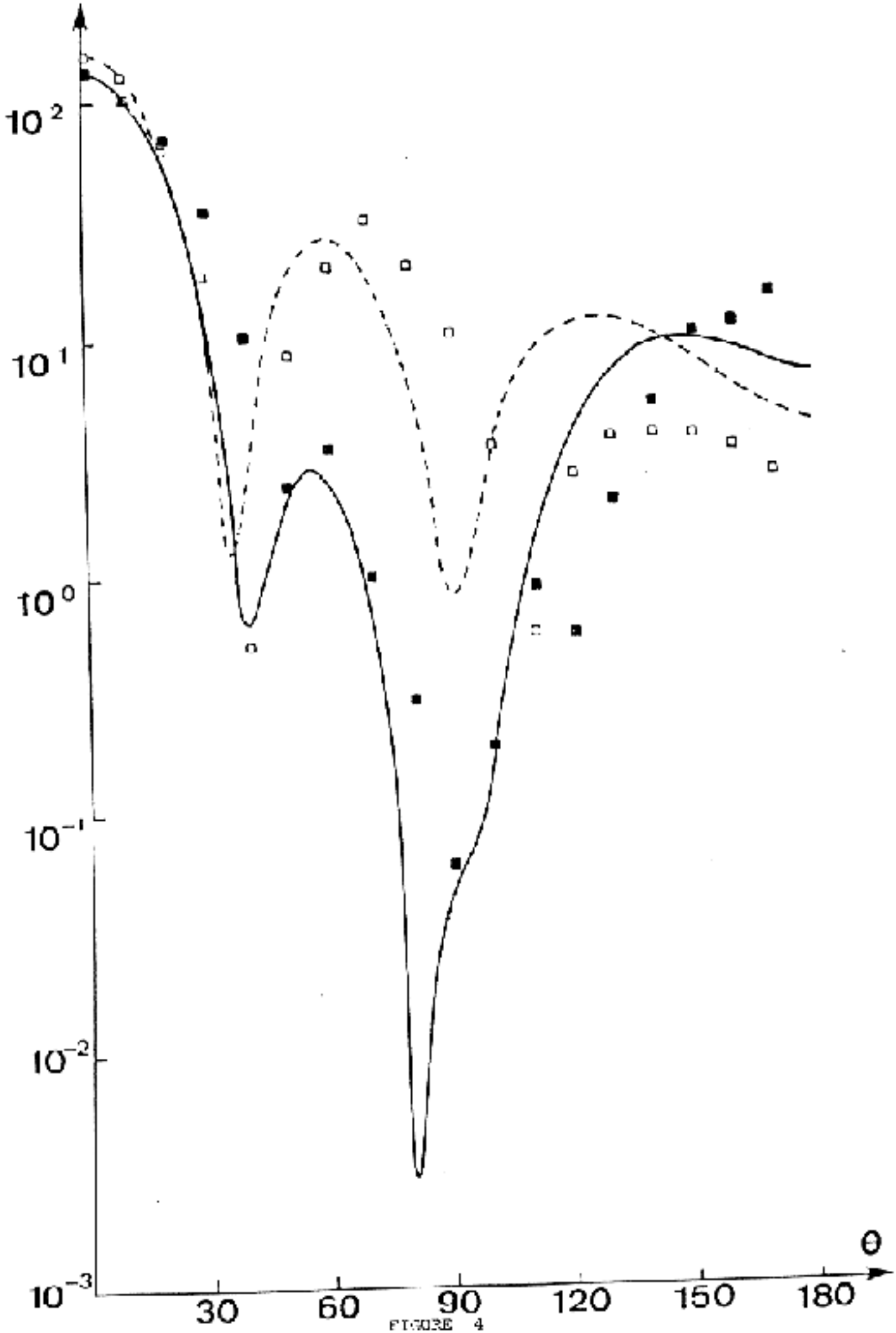

FIGURE 4

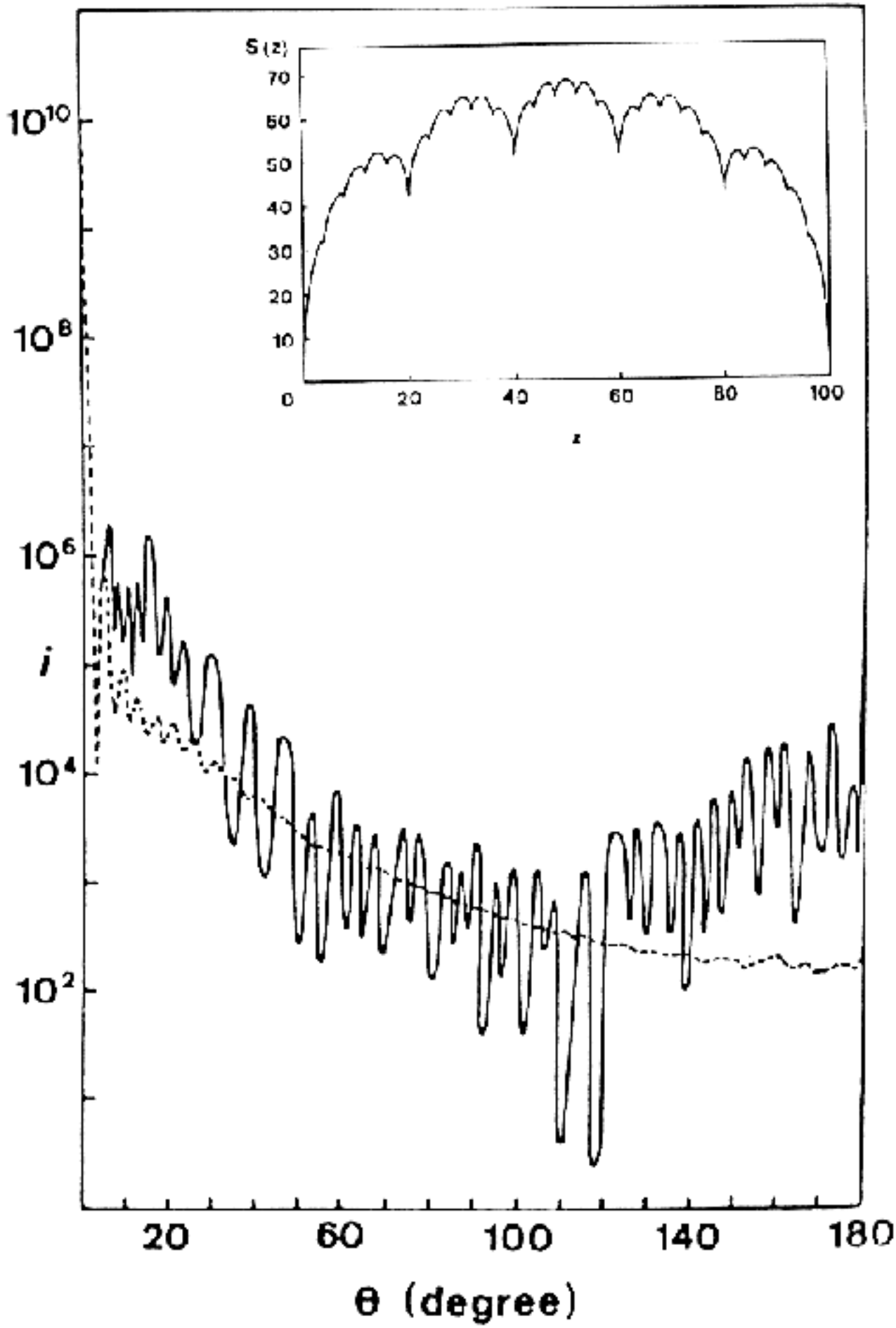
S(z)
70
60
50
40
30
20
10
0
20
40
60
80
100
z
10^{10}
10^{8}
10^{6}
10^{4}
10^{2}
i
20
60
100
140
180
θ (degree)

FIGURE 3

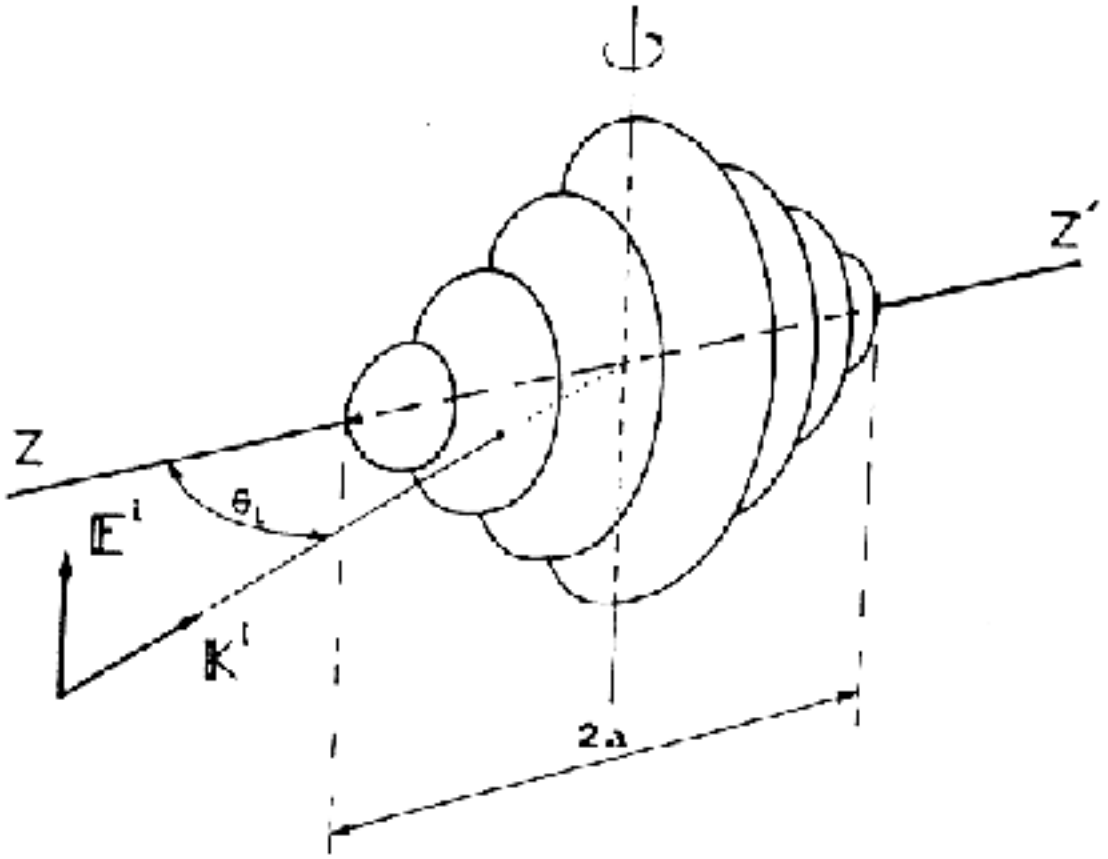

FIGURE 5

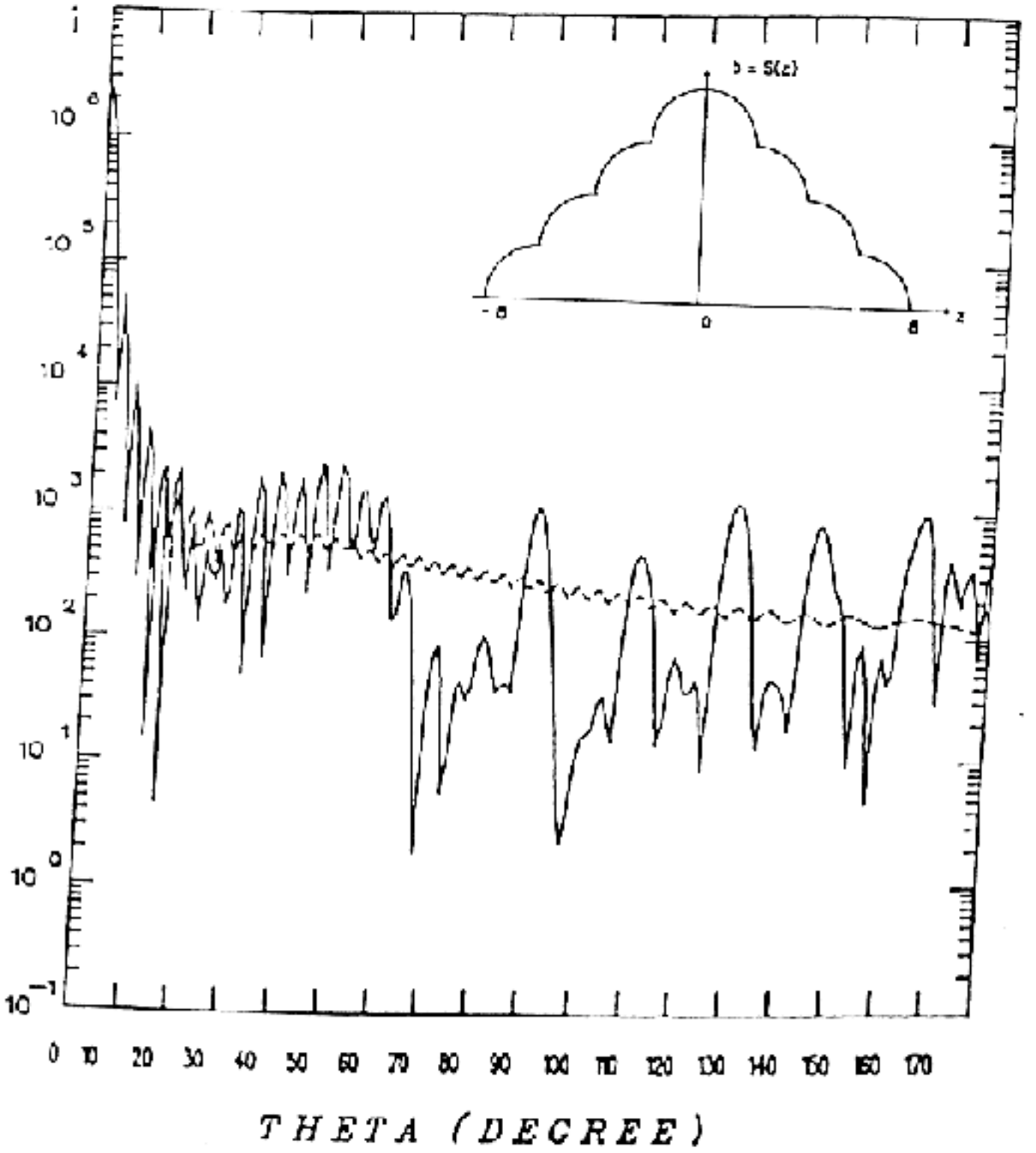
b = S(z)
-a
0
a
z
I
10^6
10^5
10^4
10^3
10^2
10^1
10^0
10^-1
0 10 20 30 40 50 60 70 80 90 100 110 120 130 140 150 160 170
THETA (DECREE)

FIGURE 7